Atmospheric Research 211 (2018) 1–11

Contents lists available at ScienceDirect

Atmospheric Research

journal homepage: www.elsevier.com/locate/atmosres

The Hamburg Tornado (7 June 2016) from the perspective of low-cost high-resolution radar data and weather forecast model

Peter Hoffmann[a,*], Claire Merker[b,c], Katharina Lengfeld[d], Felix Ament[b]

[a] Department of Mathematics, University of Hamburg, Hamburg, Germany
[b] Meteorological Institute, University of Hamburg, Hamburg, Germany
[c] MeteoSwiss, Zürich, Switzerland
[d] Deutscher Wetterdienst, Offenbach am Main, Germany

ARTICLE INFO

Keywords:
Tornado
Weather forecast
X-band radar
Numerical modelling
CCAM

ABSTRACT

A tornado hit the northeastern suburbs of Hamburg, Germany, on 7 June 2016. It had an estimated strength of upper end F1 on the Fujita scale and was short-lived with an approximate duration of only 13 min and a path length of just about 1.3 km. We demonstrate that such a small-scale, extreme event can be observed and forecasted accurately by a low-cost radar and by an atmospheric model with low computational costs, respectively.

Observations from a low-cost single polarized X-band radar covering the urban area of Hamburg with 60 m spatial and 30 s temporal resolution are analyzed with respect to their ability to capture the development as well as the track of the tornado. In contrast to the national C-band radar network, the X-band radar is capable of capturing the hook echo of the tornado as well as the circular pattern in rain rates, because of its higher resolution in space and time.

High-resolution forecasts of the tornado event are conducted with the computational efficient Conformal Cubic Atmosphere Model (CCAM) in order to test the capability of predicting the tornado with a lead time of a few hours. A three step downscaling method is used to obtain a spatial resolution of 1 km with initial conditions taken from the NCEP analysis. Calculated severe weather indices clearly indicate a potential for a tornado. CCAM cannot explicitly resolve small scale tornadic features but the model simulates a strong convective cell only a few kilometers apart from the tornadic thunderstorm observed by the radar.

1. Introduction

Tornadoes are one of the most extreme weather phenomena. Within the funnel of a tornado wind speeds of up to 135 m s^{-1} (486 km h^{-1}) occur (Alexander, 2010). Such extreme winds can cause damage to man-made structures and can lead to loss of life. Especially in urban areas with high population and building density tornadoes can be devastating. In 2011 a tornado hit Joplin, MO, United States (US), causing 158 direct fatalities and total property damage of more than two billion dollars (Marshall et al., 2012). On 20 May 2013, a tornado affected the cities of Newcastle, Moore and Oklahoma City, OK, US, resulting in 24 fatalities and more than 4250 damaged structures (Burgess et al., 2014). Although less frequent than in the US deadly and devastating tornadoes occur in Europe as well: On 9 June 1984 Russia was hit by an F4 tornado, on 8 July 2015 another F4 tornado occurred in Mira, Italy and on 12 August 2002 an F3 tornado occurred in southeastern Romania (Finch and Bikos, 2012; Lemon et al., 2003). Despite reports of 5478 tornadoes in 42 European countries causing 316 fatalities, 4462 injuries and approximately €1 billion in damages, tornadoes are still an underestimated threat in Europe (Antonescu et al., 2017). But because of their relatively low frequency of occurrence in Europe, there is a lack of knowledge and adequate tools for forecasting tornadoes (e.g. high-resolution radar networks as the one used in this study). Therefore, detecting and forecasting tornadoes remains a challenge for researchers and forecasters.

Even with the computing power of state-of-the-art supercomputers, predicting the correct timing and location of such a small-scale event is limited to a few minutes (Bluestein et al., 2007). Current operational weather forecast models reach horizontal resolutions of up to 1.5 km (Tang et al., 2013) and are able to simulate supercells (e.g. Curic and Janc, 2012; Stratman and Brewster, 2017), from where most tornadoes evolve (Davies-Jones, 2015). However, in order to resolve a tornado with a numerical model, very high resolutions of about 10 m are necessary. Such simulations pose a high demand on computing power and on data storage and are therefore not feasible for forecast purposes. In addition, the ability to forecast tornadoes is not only limited by

* Corresponding author.
E-mail address: peter.hoffmann@uni-hamburg.de (P. Hoffmann).

https://doi.org/10.1016/j.atmosres.2018.04.009
Received 31 December 2017; Received in revised form 5 April 2018; Accepted 11 April 2018
Available online 08 May 2018

Fig. 1. Footage of the tornado during different phases.
Source: (Courtesy of Frank Boettcher, Institut für Wetter- und Klimakommunikation).

computing constrains but also by the lack of complete understanding of tornado formation. According to the current understanding, the genesis of supercell tornadoes is a three stage process (Davies-Jones, 2015): 1) Formation of a rotating updraft aloft. 2) Development of a cyclone at the ground. 3) Formation of the tornado (collapse and spin-up of the above cyclone). However, based on data from the US only 26% of supercells produced a tornado (Trapp et al., 2005). Hence, severe weather indices are computed (e.g. the convective available potential energy, CAPE, wind shear) from kilometer-scale forecast models to assess the potential for a tornadic event (e.g. Gallo et al., 2016, 2018; Avgoustoglou et al., 2017), which is known as the ingredients-based approach. Based on proximity soundings or numerical weather prediction output, environments favorable for tornadoes were identified and multiple indices developed (e.g. Craven and Brooks, 2004; Thompson et al., 2003, 2012; Púčik et al., 2015).

Precipitation estimates from radar observations serve as input for weather forecast models (e.g. Stephan et al., 2008). In contrast to in-situ rain gauges, weather radars cannot observe precipitation directly, but measure the reflectivity from raindrops. Radar reflectivity has to be converted into rain rate using a common statistical relation between both quantities (e.g. Marshall and Palmer, 1948; Ulbrich and Atlas, 1978; Atlas et al., 1999). However, clear advantages of radar observations over point measurements from rain gauges are the areal coverage and the detailed information not only on the temporal but also on the spatial structure of rain events. This information is crucial to investigate and forecast tornadoes or similar weather phenomena. Radar networks of most national weather services operate in the C- or S-band frequency range and provide observations with a maximum range of several 100 km, a spatial resolution of typically 250 m–1 km and a temporal resolution in the order of 5 min. The radar network of the German Meteorological Service (DWD) e.g. has recently been upgraded to polarimetric systems that provide precipitation fields with 250 m spatial resolution, but it still lacks high temporal resolution. Small-scale extreme weather phenomena such as tornadoes, however, occur very localized and on short time scales and might not be covered in sufficient detail by this kind of radar systems (Wurman and Gill, 2000).

High-resolution X-band weather radars can give more detailed information on temporal and spatial structure as well as evolution of precipitation events. These systems can operate with resolution of less than 1 min in time and a few 10 m in space. Mobile Doppler X-band radars have been used for detection and investigation of the evolution of several tornadoes that occurred in the last decade, e.g. in the US (French et al., 2014; Tanamachi et al., 2012) and the Netherlands (Akerboom, 2016). Dawson et al. (2017) demonstrated that data from Doppler X-band radars with coarser resolution can be used to verify supercell forecasts. However, dual-polarized Doppler systems are costly and the interpretation of the observations requires experienced staff. A less expensive and simpler alternative is the usage of single-polarized ship navigation radars adapted to the requirements of precipitation observation. In Hamburg, Germany, such a single-polarized low-cost X-band radar provides rainfall observations every 30 s with a spatial resolution of 60 m and 1° that allows for detailed information about the spatial and temporal evolution of precipitation events in the urban area (Lengfeld et al., 2014). Single-polarized X-band radar measurements have been shown to detect tornado echoes previously (Sutherland-Stacey et al., 2010).

On 7 June 2016 parts of Hamburg were hit by a weak tornado. This was already the third confirmed tornado that occurred within the city boundaries of Hamburg in a 10 years period. Depending on the source, only 4 (European Severe Weather Database, Dotzek et al., 2009) to 6 tornadoes (Tornadoliste, 2017) were confirmed in the 50 year period before 2006 (1956–2005). In contrary to the tornado that hit Hamburg in 2006 (27 March), no injuries or fatalities were caused even though it touched ground in a populated area. Due to the higher population density in the affected area and the development of smart phones a higher number of eye witness reports, photos and videos of the 2016 tornado exist compared to the 2006 tornado (Fig. 1).

This paper will introduce an approach to examine and forecast a tornado at relatively low costs using a state-of-art radar system and nowcasting model. The high-resolution precipitation fields provided by the X-band radar that covers the urban area of Hamburg during the occurrence of the tornado and forecasts with the conformal-cubic atmospheric model (CCAM; McGregor, 2005a,b; McGregor and Dix, 2008) at a 1 km horizontal resolution will be examined. The X-band radar is introduced in Section 2. Section 3 deals with the forecast model CCAM and its set-up. The synoptic description of the event is given in Section 4 followed by radar observations and the results of the CCAM forecast in Section 5. Summary and concluding remarks are given in Section 6.

2. Radar

In this study, two different radar systems are used to investigate the tornado in Hamburg, Germany: A C-band radar that is part of the network of the German Meteorological Service (DWD) and a local area weather radar (LAWR) operating in the X-band frequency range.

The system operating in the C-band frequency range (5625 MHz) is a dual-polarized Doppler radar and is located approximately 50 km north of Hamburg. It has a maximum range of 150 km and covers the city. Reflectivity is measured with 5 min temporal, 250 m range and 1° azimuth resolution. Here, the product containing the average of four 250 m range bins is used, leading to a range resolution of 1 km. Technical details are listed in Table 1.

The Meteorological Institute of the University of Hamburg operates a LAWR in the city of Hamburg. It has a maximum range of 20 km and is set up on a rooftop in the center of Hamburg covering the whole

Table 1
Technical specifications of the X-band and C-band radar systems.

Parameters	X-band	C-band
Range resolution	60 m	250 m (product used here 1 km)
Azimuth resolution	1°	1°
Time resolution	30 s	5 min
Maximum range	20 km	150 km
Calibration accuracy	± 1 dB	± 2 dB
Transmit power	25 kW	440 kW
Frequency	9410 MHz	5625 MHz
Pulse width	0.4 µs	0.8 µs
Pulse repetition frequency	800 Hz	600 Hz
Beam width	2.8°	0.93°

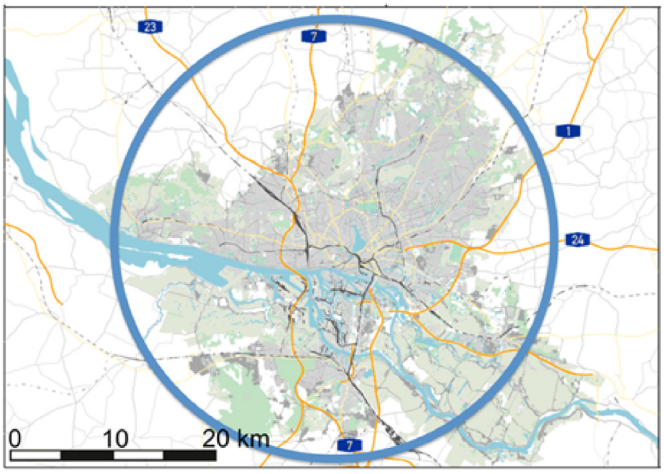

Fig. 2. Topographic map of the City of Hamburg with maximum range of the X-band radar indicated by the blue circle. (For interpretation of the references to color in this figure legend, the reader is referred to the web version of this article.)

urban area (Fig. 2). The LAWR provides horizontal reflectivity scans at a fixed elevation angle of appr. 3° with continuous rotation rate of 24 rpm. Information of 12 scans is combined for precipitation observation resulting in 30 s temporal resolution. Range resolution of 60 m and angular sampling resolution of 1° in azimuth direction are chosen. The LAWR is a modified ship navigation radar (GEM Elettronica scanner SU70-25E) that cannot perform polarimetric measurements nor observe Doppler shift. For more technical information on the LAWR see Table 1.

In order to provide valuable precipitation observations a dynamic noise correction is applied to the reflectivity measurements of the LAWR separating the precipitation signal from the background noise. Furthermore, a set of clutter filters is applied to identify non-meteorological echoes including a static clutter map, common dynamic clutter filters based on the texture of logarithmic reflectivity (TDBZ) and the SPIN field (Hubbert et al., 2009) as well as a filter that makes use of the advantage of high temporal resolution. A detailed description of the data processing is given in Lengfeld et al. (2014).

The X-band radar operates at a frequency of 9410 MHz and is strongly affected by attenuation due to liquid water because the influence of attenuation is proportional to the frequency. To correct the resulting underestimation of the precipitation rate in cases of strong rainfall, a method combining less attenuated observation from the C-band radar operated by the DWD with the X-band radar measurements is applied. This method is described and examined in detail in Lengfeld et al. (2016). It allows for correcting attenuation and at the same time preserves the advantage of high-resolution rainfall estimation from the LAWR system.

3. Forecast model

The conformal-cubic atmospheric model (CCAM; McGregor, 2005a,b; McGregor and Dix, 2008) is an open source global stretched-grid non-hydrostatic numerical model. In the past, it was used both as a weather forecast model (e.g. Thatcher and Hurley, 2010) and as a regional climate model (e.g. Katzfey et al., 2016). CCAM employs a global conformal cubic grid which consists of 8 panels with an even number of grid points. Using the Schmidt transformation (Schmidt, 1977) the grid can be stretched in a way that for the central panel high resolution with nearly even grid spacing is achieved. The horizontal resolution decreases with distance to the central panel. The advantages of the stretched-grid approach compared to the conventional limited area modelling approach are that it does not require lateral boundary conditions and that it accounts for the interactions between large-scale and small-scale processes. The disadvantages of the increased number of horizontal grid points and the non-uniform grid spacing are tackled with efficient and robust numerical schemes. The forecast, conducted for this study, was run on a Windows laptop using two processors

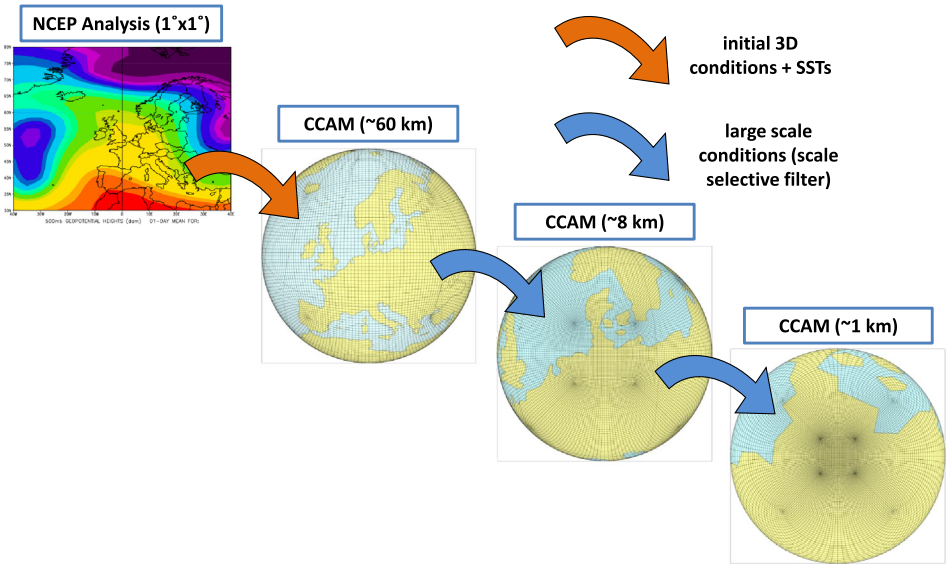

Fig. 3. CCAM forecast strategy.

within 3 h.

For the forecast of the tornadic event a three step downscaling method with a final resolution of 1 km over the Hamburg area is used (Fig. 3). In the first step, a slightly stretched version of CCAM (~60 km central panel) is initialized with atmospheric data and sea surface temperatures from the 00 UTC NCEP analysis. For the initialization of the soil variables, fields from the previous forecast run are taken. The results of this coarse forecast are used to force a second version of CCAM with stronger stretching (~8 km central panel). The large-scale atmospheric fields of the coarse run are transferred to the high-resolution run using a scale selective filter (Thatcher and McGregor, 2009). In the final step, the results of the 8 km CCAM forecast are further downscaled with a highly stretched version (~1 km central panel) employing the same forcing method. The microphysics scheme employed is a single-moment scheme that accounts for cloud liquid water, ice, snow, graupel and rain (Rotstayn, 1997). Stratman and Brewster (2017) showed that, while the forecast of tornadic supercells can be sensitive to the microphysics scheme, single-moment schemes perform reasonably well compared to multi-moment schemes. In addition, effects of aerosols on the radiation and on the cloud microphysics are considered (Rotstayn and Lohmann, 2002; Rotstayn et al., 2011), which are shown to be important for the simulations of severe convective storms (Lompar et al., 2017). In order to account for processes within the urban canopy layer, CCAM employs a state-of-the-art urban parameterization based on the Town Energy Budget (TEB; Masson, 2000), approach denoted here as aTEB (Thatcher and Hurley, 2012; Luhar et al., 2014; Lipson et al., 2017), which is coupled to the Community Atmosphere Biosphere Land Exchange model (CABLE) land-surface scheme (Kowalczyk et al., 2013). Compared to the original approach by Masson (2000) aTEB has an improved representation of suburban areas, an in-canyon vegetation parameterization, an additional parameterization for air-conditioning and an improved thermal conduction model. Accounting for urban effects is particular important because Hamburg is shown to have an impact on the precipitation distribution (Schlünzen et al., 2010). The model set-up is summarized in Table 2.

4. Event description

On 7 June 2017 an Omega blocking pattern, which slowly weakened, influenced most parts of Western and Central Europe. Within this large scale weather pattern, the surface weather chart at 12 UTC (Fig. 4) shows several short-wave troughs over Central Europe, which resulted in a convergence zone (CZ) spanning from Central France to Southern Denmark. This CZ moved slowly eastward and passed Hamburg later that day leading to a wind shift from SE to N. The objective weather type classification for Germany from the DWD based on upper air meteorological fields from the DWD forecast model (Bissolli and Dittmann, 2001) yielded the weather type XXAAW (no prevailing wind direction, anticyclonic in 950 hPa and 500 hPa, wet troposphere) for the 7 June 2016. A climatological analysis of tornadoes in Germany by Bissolli et al. (2007) shows that under such synoptic scale conditions tornado events were reported in the past while this weather type only accounts for a small portion of the tornadoes in Germany (appr. 2%).

Surfaces temperatures and dew points within and in the vicinity of Hamburg at 12 UTC ranged from 25 °C to 27 °C and from 10 °C to 15 °C, respectively. Sounding data from the two nearby stations Schleswig and Bergen show a deep dry layer above 700 hPa with step temperature laps rates above the boundary layer at 12 UTC (Fig. 5a, b). Also visible in Fig. 5a is a strong capping inversion at Schleswig (~925 hPa), which inhabits convection if no strong forcing is present but also helps building up convective available potential energy (CAPE). At 12 UTC, moderate CAPE values of 392 J kg^{-1} are present. They were likely to increase during the afternoon hours due to an increase in surface moisture (e.g. dew points at Hamburg-Fuhlsbüttel: 13 °C at 12 UTC, 17 °C at 16 UTC). At Bergen, the 12 UTC sounding shows a weaker capping inversion as well as smaller CAPE values of 30 J kg^{-1} (Fig. 5b). The additional 18 UTC sounding at Bergen (Fig. 5c), which was approximately the time when the CZ passed this station, reveals that the capping inversions disappeared as the boundary layer depth increased and that the CAPE values increased to 396 J kg^{-1}, which is comparable to the values from Schleswig at 12 UTC. However, for Hamburg CAPE values at the time of the tornado were likely higher because of higher surface moisture (17 °C vs. 14 °C for Berger at 12 UTC). The upper air winds show only weak variations with height for Schleswig (Fig. 5a) except for a low-level jet (LLJ) in 860 m above ground. The latter, is also observed at the station Norderney, located 190 km west of Hamburg and therefore west of the CZ (not shown). Up to a height of about 6 km above ground the atmosphere above Bergen at 18 UTC is almost calm (Fig. 5c). Consequently, the deep level vertical wind shear (e.g. between the surface and 6 km) needed for the development of a supercell originated not by the large scale circulation but by the varying winds along the CZ. Also the low-level wind shear (e.g. between the surface and 1 km) needed for the development of a tornado originates mostly from the CZ and to a lesser extend from the LLJ that was present in the environment west of the CZ.

The combination of the warm and moist boundary layer, the unstable layer above, and the CZ as a lifting mechanism led to widespread thunderstorm development over Western and Northern Germany in the afternoon. One of the cells that developed in the area of Hamburg evolved into a supercell. At around 16:24 UTC (18:24 CEST), the tornado touched ground in the suburb of Bramfeld. With an approximate duration of 13 min and a path length of appr. 1.3 km the tornado was short-lived. It caused only moderate damage and fortunately no fatalities or injuries. Based on the damage reports, the strength of the tornado is estimated to be F1 (upper end) on the Fujita scale (Tornadoliste, 2017), which indicates wind speeds between 33 m s^{-1} to 50 m s^{-1}. However, no official classification was conducted for this tornado.

Table 2
Set-up of the CCAM simulations.

Nesting	Scale selective filter (Thatcher and McGregor, 2009)
Horizontal grid	C48 (48 × 48 × 8)
Midpoint of central panel	9.99 ° East, 53.63 °North
Schmidt factor (resolution central panel)	3.33 (~60 km); 25 (~8 km); 200 (~1 km)
Vertical levels	27
Urban scheme	aTEB (Thatcher and Hurley, 2012)
Cloud microphysics scheme	Cloud liquid water, ice, snow, graupel and rain (Rotstayn, 1997)
Aerosol scheme	(Rotstayn and Lohmann, 2002; Rotstayn et al., 2011)
Short-wave and long-wave radiation	Updated GFDL parameterizations (Schwarzkopf and Ramaswamy, 1999; Freidenreich and Ramaswamy, 1999)
Cumulus convection scheme	Mass-flux closure (improved version based on McGregor, 2003)
Initial conditions	NCEP analysis 1° × 1°
Land surface scheme	CABLE (Kowalczyk et al., 2013)

5. Results

5.1. Radar

The LAWR covering the area of Hamburg first detected the cell from which the tornado developed around 15:20 UTC. The cell intensifies over the next hour but stays quasi-stationary east-north east of Hamburg (Fig. 6). From 16:14:30 UTC on, radar signal indicates the development of a tornado. The characteristic hook echo is visible between 16:20:30 UTC and 16:28:30 UTC. During this time interval, the LAWR captures a circular hook echo in the rain rate. It can be attributed to precipitation occurring in the clouds rotating around the tornado (i.e. wall cloud). Fig. 7 shows a detail of Fig. 6e together with the tornado

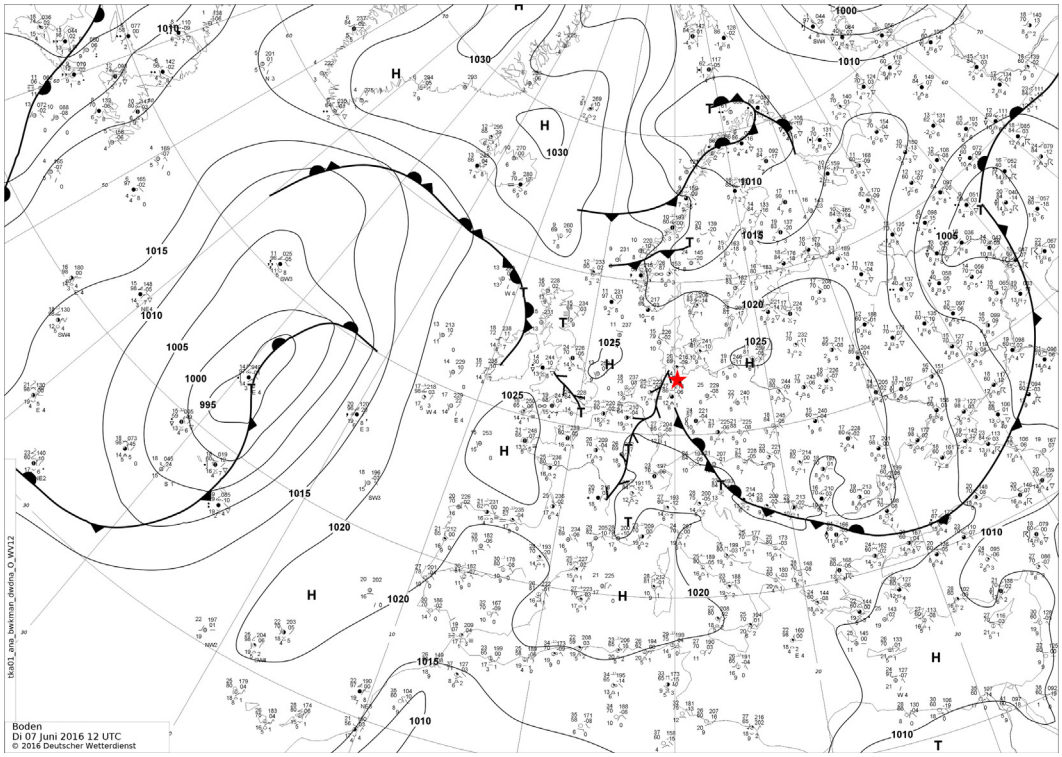

Fig. 4. Surface weather chart for 7 June 2016 12 UTC prepared by the German Meteorological Service (DWD). Hamburg is marked with a red star. (For interpretation of the references to color in this figure legend, the reader is referred to the web version of this article.)

track at ground, reconstructed from reports on damage observations. Since reconstructed after the event, the tornado track does not include time information. The shift between the tornado track at ground and the wall cloud signal at radar height is probably due to an inclination of the tornado funnel (Fig. 1). Maximum recorded reflectivity during the event is 69.7 dBZ at 16:29:30 UTC, which corresponds to 474 mm h^{-1} for this 30 s value. It occurs after the tornado is recorded in the part of the cell intensifying north east of the tornado location. Accumulated hourly rainfall for 16:00:00 UTC, 17:00:00 UTC, and 18:00:00 UTC (Fig. 8) confirm the local development of the precipitating cell before 16:00:00 UTC. Due to the stationary position of the cell, precipitation between 16:00:00 and 17:00:00 UTC sums up to a maximum of 39 mm. Between 17:00:00 UTC and 18:00:00 UTC, the area of the signal of the cell within radar reach decreases, but accumulated rain fall increases to 53 mm.

Data of the C-band radar operated by DWD at the Boostedt site also clearly shows the stationary precipitation cell in the northeast of Hamburg (Fig. 9). A hook echo is apparent in the data at 16:20:30 UTC, but the signal is indistinct and not visible in the time steps before and after. Therefore, the tornado is not discernible in the C-band reflectivity data. Though, the C-band radar network of DWD also provides Doppler information in which the tornado is visible.

5.2. CCAM

The simulation results of the finest version of CCAM are discussed in the following. In the applied version of CCAM only hourly accumulated rainfall is available (Fig. 10). Consequently, CCAM rainfall can only be compared to the hourly rainfall sums in Fig. 8. Multiple small convective cells can be seen northwest of Hamburg at 16 UTC (Fig. 10a) that intensify and merge into a large cell at 17 UTC (Fig. 10b). This corresponds to the tornado producing cell seen in the radar data (Fig. 8b). It is however shifted to the west compared to the radar data. Hence, the tornado track is missed by a few grid cells. With a maximum hourly averaged rainfall rate within the cell of 19 mm h^{-1} CCAM underestimates the rainfall intensity by 50% compared to the X-band radar. This is likely due to the lower spatial resolution of CCAM (~1 km). In addition, Lompar et al. (2018) suggested that by including gust front scheme higher cumulative rainfall amounts can be expected. At 19 UTC, the convective activity weakened but the cell only slowly moved eastwards (Fig. 10c). The propagation speed is slower than observed and some smaller cells are visible that are not present in the radar data.

It is not possible to forecast a tornado with analyzing simulated rainfall or wind at a kilometer-scale resolution. Therefore, similar to Das et al. (2016) severe weather indices, which are used to assess the probability of a tornadic event, are computed from the CCAM forecast. There is a wide range of such indices available in the literature and the use of such indices depends on the preferences of the forecaster. Here, we only show three indices that are used by the Storm Predication Center (SPC) and that are easy to compute and interpret. In the following we will first define these indices and then present the analysis of the tornado event.

5.2.1. Convective available potential energy

One of the widely used thermodynamic indices is CAPE, which is a measure for convective potential of the atmosphere. It can be directly linked to the vertical wind speed within a convective updraft and hence the strength of a thunderstorm. CAPE is calculated by vertically integrating the buoyancy of an air parcel from the level of free convection z_{fc} to the equilibrium level z_{el}:

$$CAPE = \int_{z_{fc}}^{z_{el}} g \frac{(T_{vp} - T_{vs})}{T_{vs}} dz, \tag{1}$$

where g is the gravitational constant, T_{vp} the virtual temperature of the air parcel and T_{ve} the virtual temperature of the environment. There are many different types of CAPE, depending on which parcel is chosen. Examples are the surface based CAPE (SBCAPE), the most unstable CAPE (MUCAPE) and the mixed layer CAPE (MLCAPE). All these types

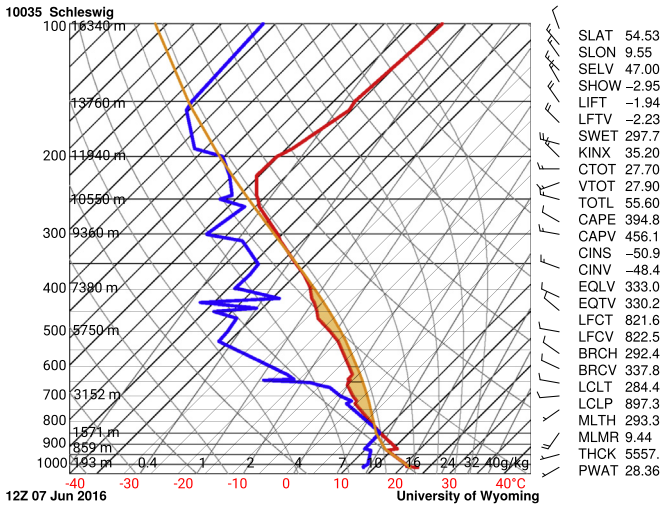

(a)

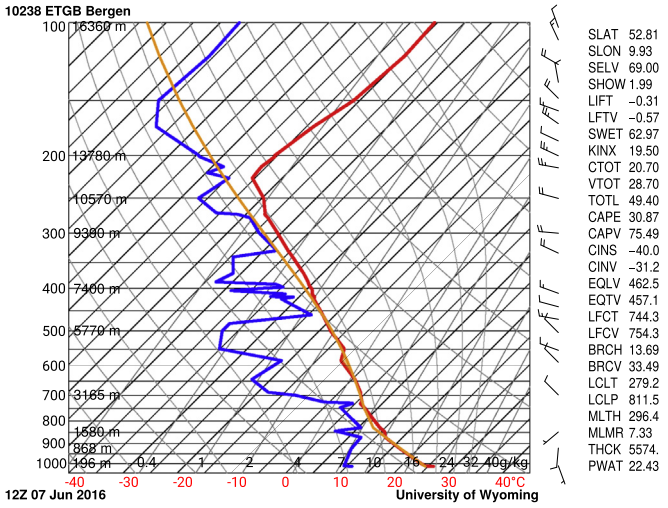

(b)

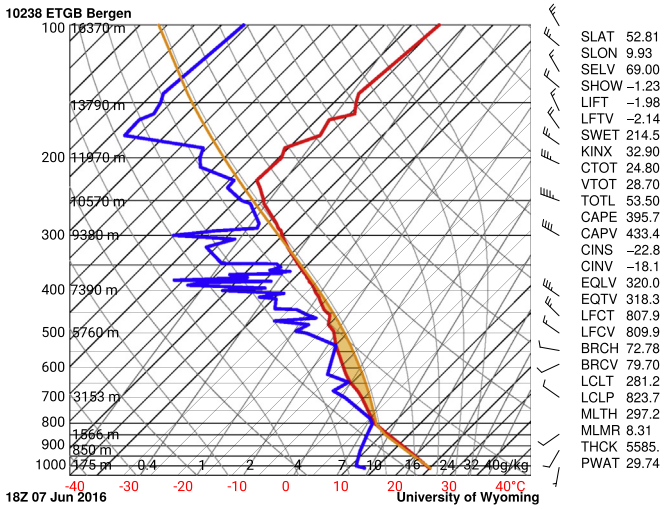

(c)

Fig. 5. Skew-T charts of the 7 June 2016 12 UTC sounding data from a) Schleswig (ca. 110 km north of Hamburg), b) Bergen (ca. 80 km south of Hamburg) and c) 18 UTC sounding from Bergen. Red and blue lines indicate the environmental temperature and dew point temperature, respectively. The temperature of the air parcel used to compute CAPE is indicated by the orange line. The light orange area between the red line and the orange line corresponds to CAPE. (For interpretation of the references to color in this figure legend, the reader is referred to the web version of this article.)
(Source: Department of Atmospheric Science, University of Wyoming; color and thickness of lines and font size have been modified).

of CAPE differ primarily in the starting height of the parcel. CCAM computes CAPE for each time step as part of the convection parameterization. Similar to the computation of MLCAPE, T_{vp} is computed as an average over the mixed-layer but instead of z_{fc} and z_{el} the level of the cloud base and the limit of moist static instability, respectively, are used (McGregor, personal communication). In addition, entrainment and detrainment processes are included, which might lead to lower values of CAPE compared to MLCAPE. The latter, assumes no mixing between the ascending air parcel and the surrounding environment. In the current version of CCAM, CAPE is only saved for grid cells where convection occurred. As output variables average CAPE (averaging time step 1 h) and maximum CAPE are available. In order, to identify the potential for a severe tornadic thunderstorm the latter is used.

5.2.2. Vertical wind shear

As mentioned in Section 4, vertically varying winds are needed for the development of supercells and tornadoes. The difference between wind vectors $\vec{v}$ in different heights is called vertical wind shear. It is usually computed between two fixed heights. While for the development of supercells deep-level wind shear (DLS; e.g. 0–6 km) is important, the formation of tornadoes is associated with low-level wind shear (LLS; e.g. 0–1 km). Based on the guidelines of the SPC (SPC, 2017) an environment with LLS between surface and 1 km above 15–20 kts (7.7 m s^{-1} to 15.4 m s^{-1}) is favorable for tornado development while supercells are commonly associated with DLS of 35–40 kts (18 m s^{-1} to 20.5 m s^{-1}). In CCAM, vertical wind shear can be easily obtained by subtracting the wind vectors near the surface and at fixed heights (Eqs. (2) and (3)), which were interpolated from CCAM's sigma coordinates.

$$LLS = |\vec{v}\,(0\ \text{km}) - \vec{v}\,(1\ \text{km})| \tag{2}$$

$$DLS = |\vec{v}\,(0\ \text{km}) - \vec{v}\,(6\ \text{km})| \tag{3}$$

5.2.3. Significant severe index

For the development of supercells thermo-dynamic and dynamic atmospheric conditions need to be present at the same time. Hence, forecasters use combined indices to find areas with a potential for severe thunderstorms. One of these indices was introduced by Craven and Brooks (2004). They combined deep-level shear and MLCAPE into one index (Eq. (4)). Based on proximity soundings of severe weather events, they found that significant severe weather (hail = 2 in. and wind gusts = 65 kts) and significant tornadoes (F2 and above) are likely to occur if the product of both parameters is above 20· 10^3 m^3 s^{-3} and 30· 10^3 m^3 s^{-3}, respectively. In this study, this index is referred to as significant severe index (SSI).

$$SSI = MLCAPE{\cdot}DLS \tag{4}$$

5.2.4. Severe weather indices in the CCAM forecast

Fig. 11 shows the three indices, CAPE, LLS and SSI, respectively, computed for 17 UTC, the time of the tornado as well as of the strongest rainfall signal in the CCAM forecast. CAPE values over Hamburg range from 1000 J kg^{-1} to more than 2000 J kg^{-1} (Fig. 11a), which show thermodynamically favorable conditions for strong thunderstorm development. Northwest and southeast of Hamburg, CAPE is zero because

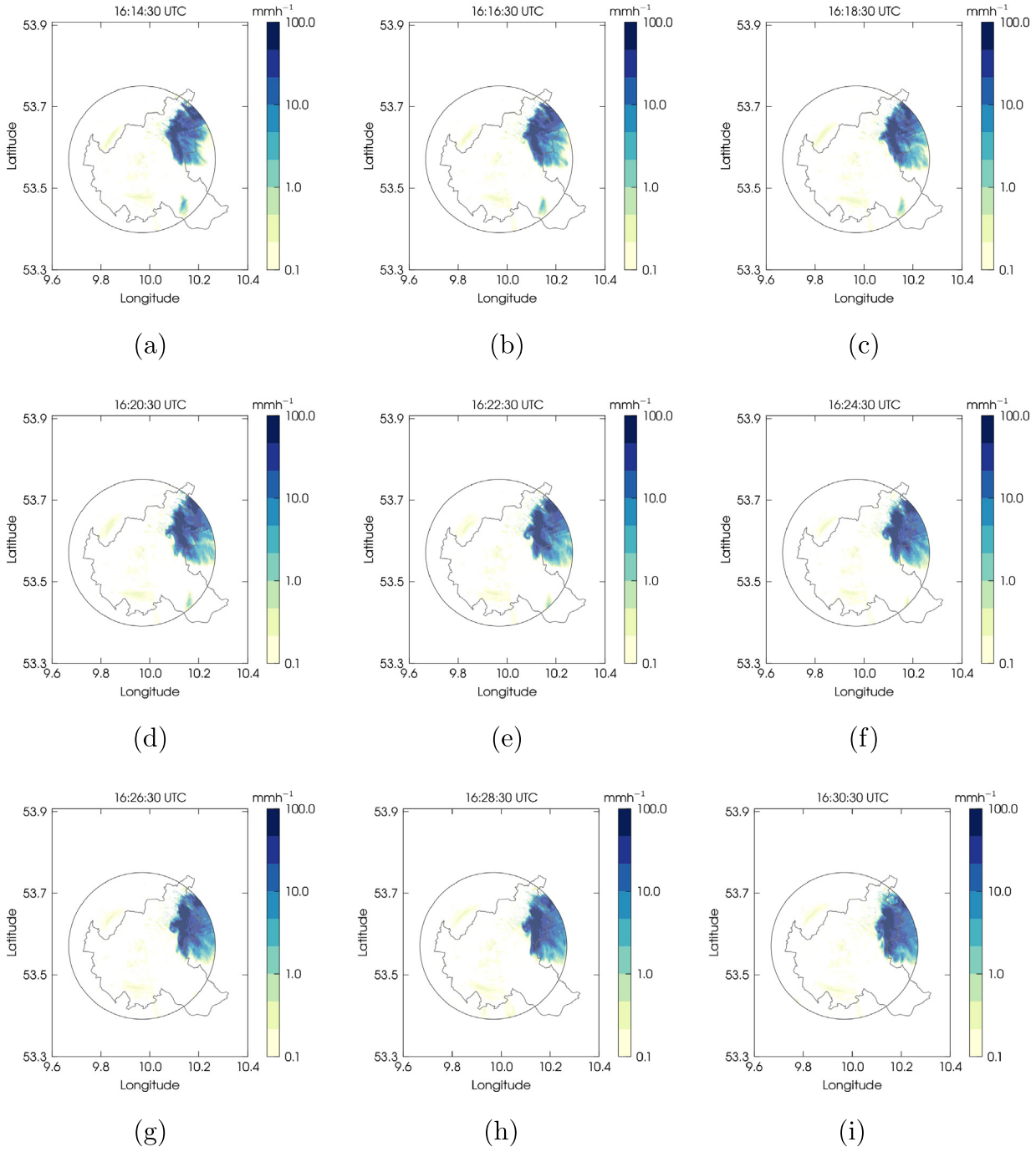

Fig. 6. Precipitation fields measured by the LAWR radar in Hamburg from 16:14:30 UTC to 16:30:30 UTC, in 2 min interval. The circle indicates the radar reach and the outline shows the political boundaries of the city of Hamburg.

CAPE is only computed in CCAM if convection occurred. Also directly over the water bodies small values of CAPE are visible due to the lower near-surface temperatures.

LLS shows high values of up to 12 m s^{-1} close to the convective cells in the norther parts of Hamburg (Fig. 11b), which indicate favorable conditions for tornado development. The maximum is located in the area of the tornado path. Over other parts of Hamburg values of low level wind shear are below 7 m s^{-1}. Hence, the larger scale conditions with respect to dynamics in the boundary layer seem to be not supportive for the tornado development. The CCAM results suggest that the LLS originated from the combination of the convective outflow and the directional shear due to the CZ.

The values for SSI range from 10· 10^3 m^3 s^{-3} to 25· 10^3 m^3 s^{-3} over most parts of Hamburg (Fig. 11c). Especially west of the strong convective cell (Fig. 10b), SSI values are larger than the threshold for significant sever weather (i.e. 20· 10^3 m^3 s^{-3}). However, they are all lower than the threshold for significant tornadoes (i.e. 30· 10^3 m^3 s^{-3}). This is due to the moderate DLS of only up to 15 m s^{-1} (not shown).

In summary, the severe weather indices discussed above indicate that the simulated thunderstorm (Fig. 10) was likely to produce severe weather phenomena such as strong wind gusts or large hail. CAPE and LLS indicate that a tornado was also likely while the SSI is not as supportive for tornado development.

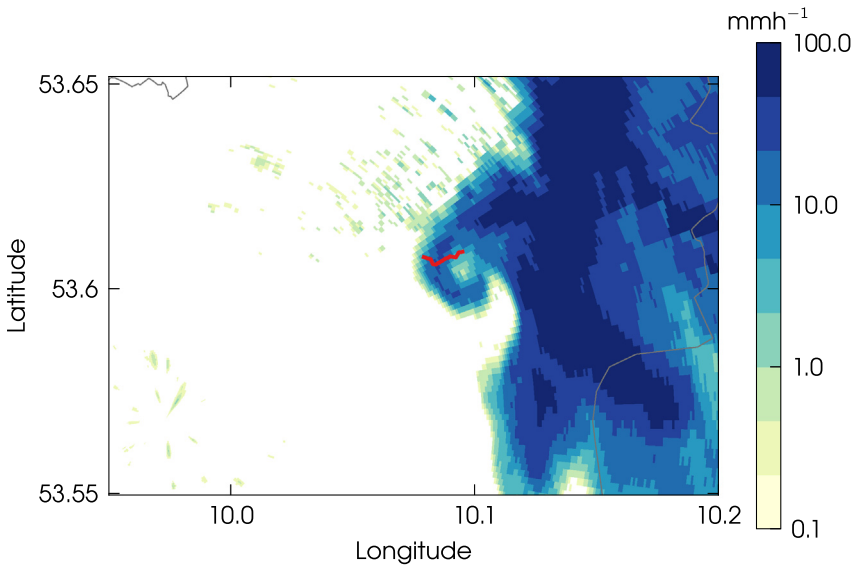

Fig. 7. Detail of the cell presented in Fig. 6e at 16:22:30 UTC. The circular pattern in the rain rate indicates the rotating circulation around the tornado. The red line indicates the tornado track as reconstructed from damage observations (path length appr. 1.3 km). (For interpretation of the references to color in this figure legend, the reader is referred to the web version of this article.)

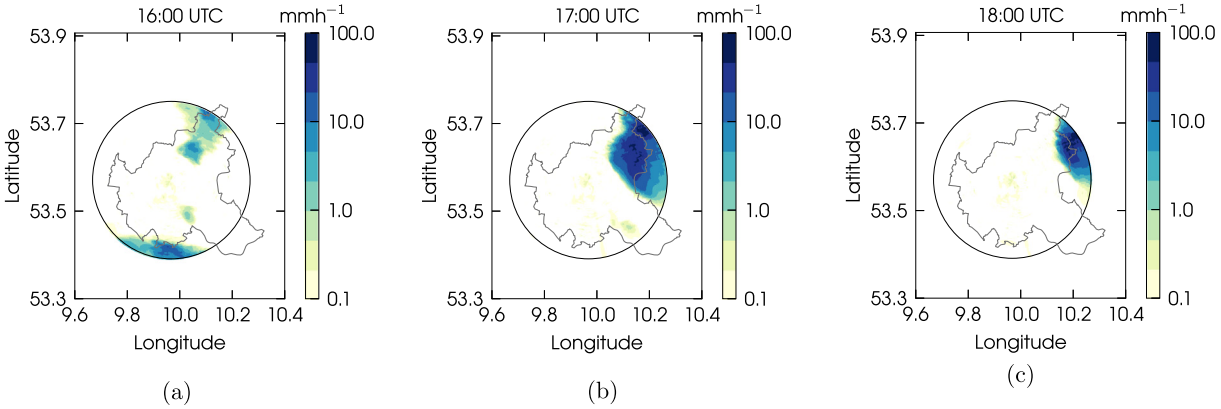

Fig. 8. Hourly precipitation sums for 07.06.2016 16:00:00, 17:00:00 and 18:00:00 UTC as seen from the LAWR in Hamburg.

6. Conclusions

On 7 June 2016 the rare event of a tornado occurred in the urban area of Hamburg, Germany. The tornado was rated F1 in the Fujita scale and despite touching ground in a highly populated area, did not cause fatalities but only property damage. In this study, we investigated the event from the observational as well as from the modelling perspective. Observations from two different radar systems that cover the urban area of Hamburg are compared: A C-band radar operated by the German Meteorological Service (DWD) and a single-polarized horizontally scanning X-band radar. The former provides precipitation estimates in 5 min temporal and 1 km range resolution, the latter in 30 s temporal and 60 m range resolution. While the C-band radar only vaguely resolved the typical tornado pattern, in the X-band radar data a clear structure of a hook echo can be seen that coincides well with the tornado track. Observations every 30 s allow for resolving the development and decline of the tornado. This underlines the importance of precipitation estimates from high-resolution radar observations for nowcasting small-scale events such as tornadoes. Especially, for urban areas a precise location of a tornado can be crucial for warning and emergency response systems.

In addition, the open-source Conformal Cubic Atmosphere Model (CCAM) is used for forecasting the tornadic event. The simulation was time saving and computationally cheap compared to forecast systems employed by national weather services because of CCAM's efficient code and because of the use of external initial conditions. Operational forecast models use some kind of data assimilation to yield initial fields. For the forecast conducted in this study, NCEP analysis data are employed for the initialization of CCAM. A comparison of hourly accumulated precipitation before, during and after the tornado indicates accordance between CCAM and rainfall estimates from the X-band radar. At the time of the tornado, CCAM simulations show a strong convective cell in the northern part of Hamburg with hourly accumulated rainfall of more than 10 mm h^{-1}. This corresponds well with radar observations although the convective cell is shifted slightly westward in the CCAM simulations. However, in the following hour CCAM simulates small convective cells in the area of the tornado that are not present in the observations.

In addition to the hourly accumulated precipitation, three indices from CCAM for possible tornadic conditions are investigated: convective available potential energy (CAPE), vertical wind shear and the significant severe index (SSI). The 0–1 km vertical wind shear at 17 UTC indicates favorable conditions for severe storm development with a maximum of 12 m s^{-1} in the area where the tornado occurred. Maximum CAPE and SSI also indicate good conditions for severe thunderstorm development with values higher than 2000 J kg^{-1} and 25· 10^3 m^3 s^{-3}, respectively. However, the areas of strongest CAPE and SSI are slightly shifted westward missing the tornado track by a few grid cells.

These results demonstrate the ability of CCAM to forecast a small-scale severe weather event, using just a small amount of computing time (3 h on a standard laptop) compared to operational forecast

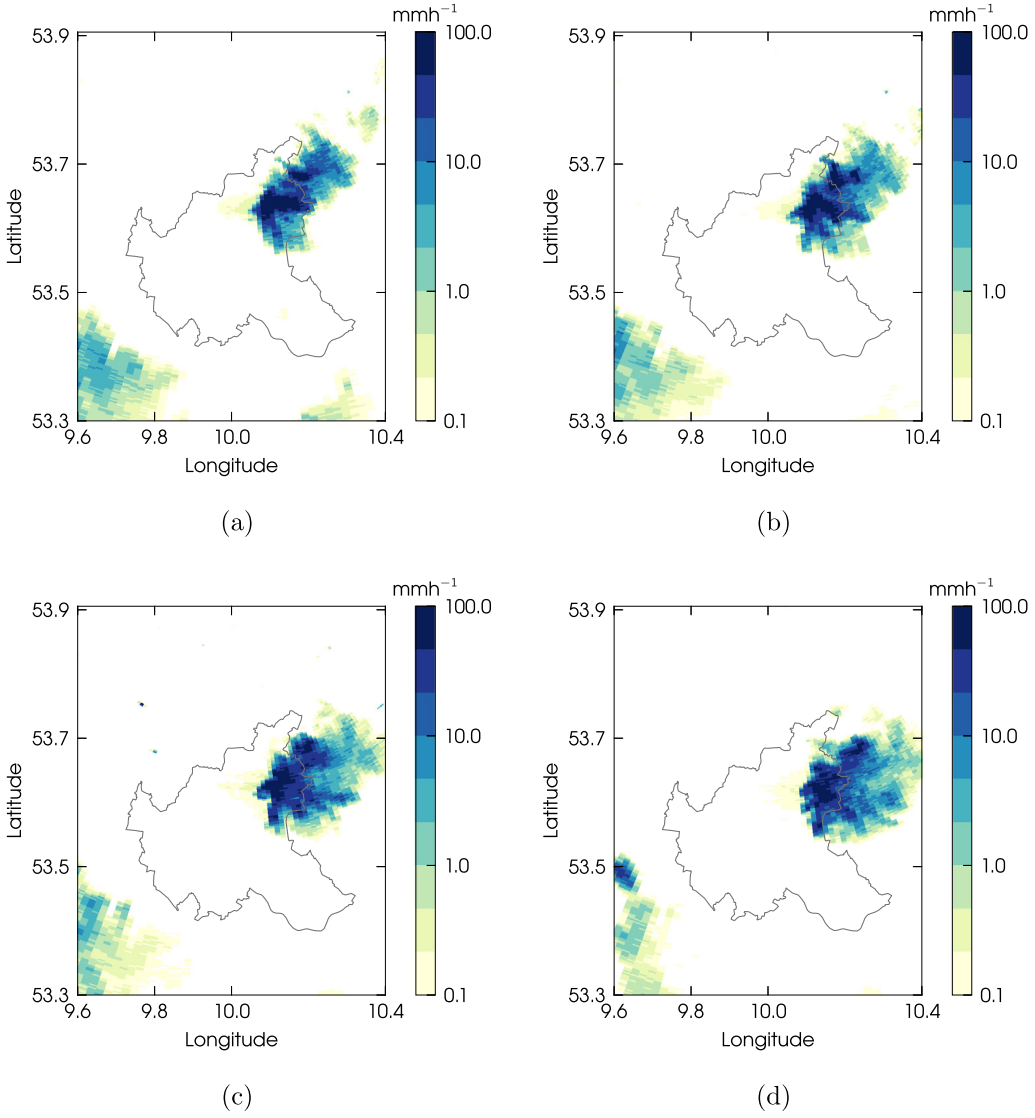

Fig. 9. Precipitation fields measured by the C-band radar in Boostedt for 16:15:30, 16:20:30, 16:25:30 and 16:30:30 UTC. (For interpretation of the references to color in this figure legend, the reader is referred to the web version of this article.)

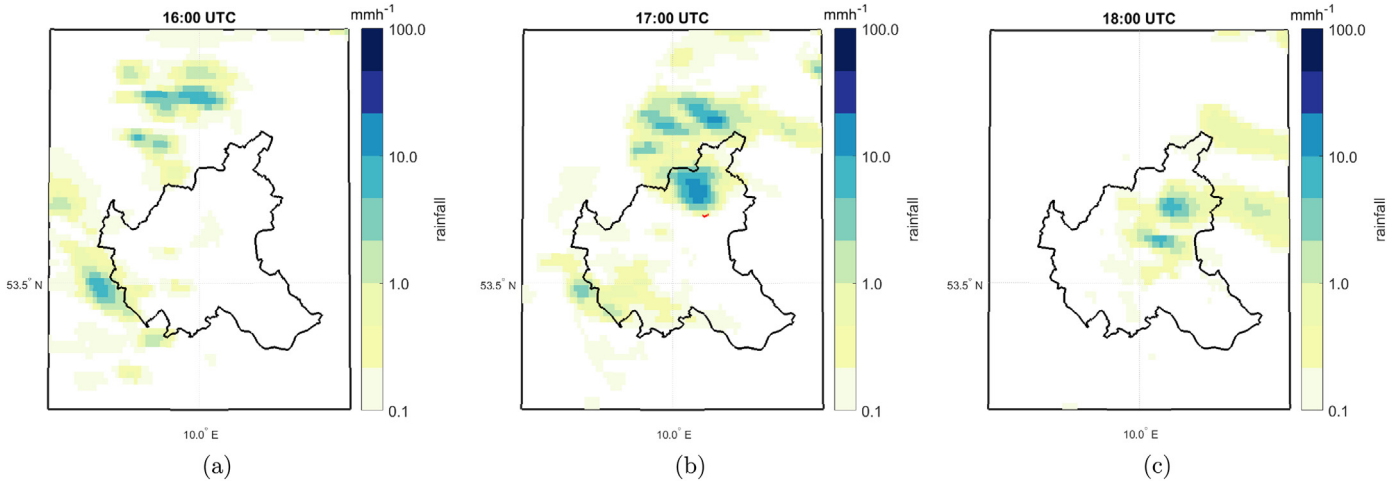

Fig. 10. Accumulated hourly rainfall of the 1 km CCAM forecast for a) 16:00 UTC, b) 17:00 UTC and c) 18:00 UTC. The red line in b) shows the tornado track. (For interpretation of the references to color in this figure legend, the reader is referred to the web version of this article.)

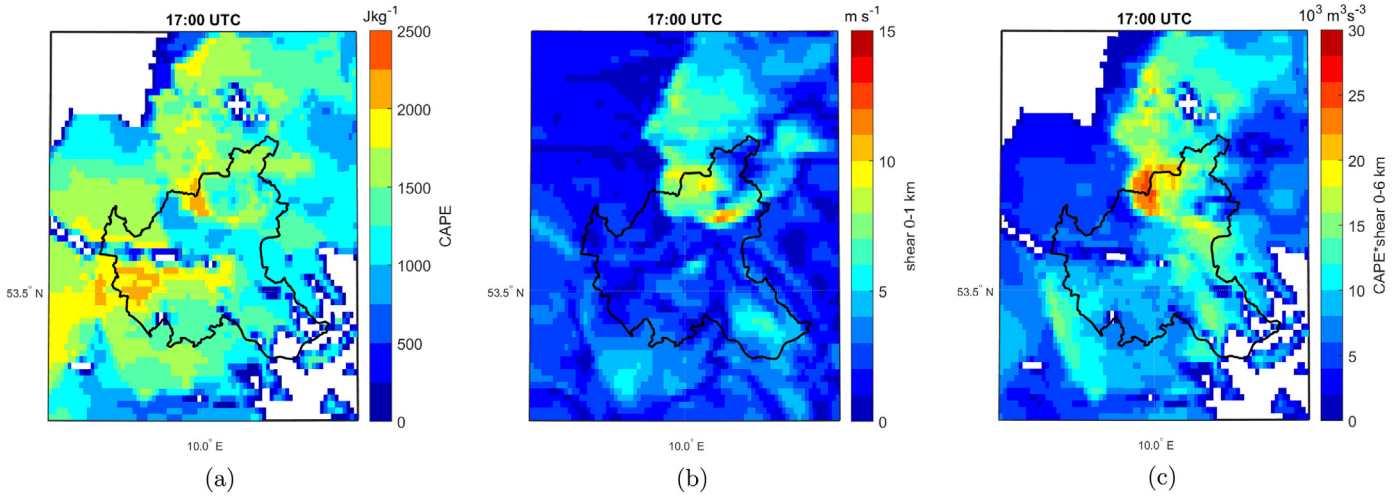

Fig. 11. Results of the 1 km CCAM forecast for a) convective available potential energy (CAPE), b) 0–1 km vertical wind shear (LLS) and c) significant severe index (SSI) by Craven and Brooks (2004) at 17 UTC.

systems. However, more comprehensive studies for a large number of such severe weather events need to be performed to quantitatively determine the forecast skill of CCAM with respect to severe weather. Nevertheless, CCAM might be a future tool for countries that do not operate very high resolution weather forecasts yet. Additionally, in combination with a system of low-cost X-band radars as a validation and nowcasting tool warning systems could be set up. To nowcast tornado favorable conditions with larger lead times, the range of the X-band radar of only 20 km is too small. A combination with observations from C-band radars could be beneficial to anticipate possible thunderstorms a few hours in advance. The higher resolved X-band radar data can then be used for nowcasting in the area of interest.

Acknowledgments

This work was partly supported by the research projects ‘Cities in Change–Development of a multi-sectoral urban development-impact model (UrbMod)’ (LFF-FV17), ‘Precipitation and Attenuation Estimates from a High-Resolution Weather Radar Network (PATTERN)’ (DFG-AM 308/1-3) and the Cluster of Excellence 'CliSAP' (DFG-EXC177). Special thanks go to Akio Hansen for providing the tornado track data, to Marcus Thatcher for providing the CCAM code and for helpful discussions, to John McGregor for information about the convection scheme, to Jack Katzfey for helping with the post-processing, and to Frank Boettcher and the Institut für Wetter- und Klimakommunikation for allowing the use of the tornado footage.

References

Akerboom, M., 2016. Tornado Detection Using a Dual Polarimetric X-Band Weather Radar in The Netherlands: A Case Study (Master thesis). Civil Engineering and Geoscience, Delft University of Technology.

Alexander, C.R., 2010. A Mobile Radar Based Climatology of Supercell Tornado Structures and Dynamics (Ph.D. thesis). University of Oklahoma.

Antonescu, B., Schultz, D.M., Holzer, A., Groenemeijer, P., 2017. Tornadoes in Europe: an underestimated threat. Bull. Am. Meteorol. Soc. 98, 713–728. http://dx.doi.org/10.1175/BAMS-D-16-0171.1.

Atlas, D., Ulbrich, C.W., Marks, F.D., Amitai, E., Williams, C.R., 1999. Systematic variation of drop size and radar-rainfall relations. J. Geophys. Res. Atmos. 104, 6155–6169. http://dx.doi.org/10.1029/1998JD200098.

Avgoustoglou, E., Matsangouras, I., Pytharoulis, I., Kamperakis, N., Mylonas, M., Nastos, P., Bluestein, H., 2017. Numerical modeling analysis of the mesoscale environment conducive to two tornado events using the COSMO.Gr model over Greece. Atmos. Res. http://dx.doi.org/10.1016/j.atmosres.2017.07.022.

Bissolli, P., Dittmann, E., 2001. The objective weather type classification of the German Weather Service and its possibilities of application to environmental and meteorological investigations. Meteorol. Z. 10, 253–260. http://dx.doi.org/10.1127/0941-2948/2001/0010-0253.

Bissolli, P., Grieser, J., Dotzek, N., Welsch, M., 2007. Tornadoes in Germany 1950–2003 and their relation to particular weather conditions. Glob. Planet. Chang. 57, 124–138. http://dx.doi.org/10.1016/j.gloplacha.2006.11.007.

Bluestein, H.B., French, M.M., Tanamachi, R.L., Frasier, S., Hardwick, K., Junyent, F., Pazmany, A.L., 2007. Close-range observations of tornadoes in supercells made with a dual-polarization, X-band, mobile doppler radar. Mon. Weather Rev. 135, 1522–1543. http://dx.doi.org/10.1175/MWR3349.1.

Burgess, D., Ortega, K., Stumpf, G., Garfied, G., Karstens, C., Meyer, T., Smith, B., 2014. 20 May 2013 Moore, Oklahoma, tornado: Damahe survey and analysis. Weather Forecast. 29, 1229–1237. http://dx.doi.org/10.1175/WAF-D-14-00039.1.

Craven, J.P., Brooks, H.E., 2004. Baseline climatology of sounding derived parameters associated with deep, moist convection. Nat. Weather Dig. 28, 13–24.

Curic, M., Janc, D., 2012. Differential heating influence on hailstorm vortex pair evolution. Q. J. R. Meteorol. Soc. 138, 72–80. http://dx.doi.org/10.1002/qj.918.

Das, M.K., Das, S., Chowdhury, M.A.M., Karmakar, S., 2016. Simulation of tornado over Brahmanbaria on 22 March 2013 using Doppler weather radar and WRF model. Geomat. Nat. Haz. Risk 7, 1577–1599. http://dx.doi.org/10.1080/19475705.2015.1115432.

Davies-Jones, R., 2015. A review of supercell and tornado dynamics. Atmos. Res. 158–159, 274–291. http://dx.doi.org/10.1016/j.atmosres.2014.04.007.

Dawson, L.C., Romine, G.S., Trapp, R.J., Baldwin, M.E., 2017. Verifying supercellular rotation in a convection-permitting ensemble forecasting system with radar-derived rotation track data. Weather Forecast. 32 (2), 781–795. http://dx.doi.org/10.1175/WAF-D-16-0121.1.

Dotzek, N., Groenemeijer, P., Feuerstein, B., Holzer, A.M., 2009. Overview of ESSL's severe convective storms research using the European Severe Weather Database ESWD. Atmos. Res. 93, 575–586. http://dx.doi.org/10.1016/j.atmosres.2008.10.020.

Finch, J., Bikos, D., 2012. Russian tornado outbreak of June 1984. Electron. J. Severe Storms Meteorol. 7, 1–28.

Freidenreich, S.M., Ramaswamy, V., 1999. A new multiple-band solar radiative parameterization for general circulation models. J. Geophys. Res. Atmos. 104, 31389–31409. http://dx.doi.org/10.1029/1999JD900456.

French, M.M., Bluestein, H.B., PopStefanija, I., Baldi, C.A., Bluth, R.T., 2014. Mobile, phased-array, doppler radar observations of tornadoes at x band. Mon. Weather Rev. 142, 1010–1036. http://dx.doi.org/10.1175/MWR-D-13-00101.1.

Gallo, B.T., Clark, A.J., Dembek, S.R., 2016. Forecasting tornadoes using convection-permitting ensembles. Weather Forecast. 31, 273–295. http://dx.doi.org/10.1175/WAF-D-15-0134.1.

Gallo, B.T., Clark, A.J., Smith, B.T., Thompson, R.L., Jirak, I., Dembek, S.R., 2018. Blended probabilistic tornado forecasts: combining climatological frequencies with NSSL-WRF ensemble forecasts. Weather Forecast. 0http://dx.doi.org/10.1175/WAF-D-17-0132.1. null.

Hubbert, J.C., Dixon, M., Ellis, S.M., Meymaris, G., 2009. Weather radar ground clutter. Part I: Identification, modeling, and simulation. J. Atmos. Ocean. Technol. 26, 1165–1180. http://dx.doi.org/10.1175/2009JTECHA1159.1.

Katzfey, J., Nguyen, K., McGregor, J., Hoffmann, P., Ramasamy, S., Nguyen, H.V., Khiem, M.V., Nguyen, T.V., Truong, K.B., Vu, T.V., Nguyen, H.T., Thuc, T., Phong, D.H., Nguyen, B.T., Phan-Van, T., Nguyen-Quang, T., Ngo-Duc, T., Trinh-Tuan, L., 2016. High-resolution simulations for Vietnam - methodology and evaluation of current climate. Asia-Pac. J. Atmos. Sci. 52, 91–106. http://dx.doi.org/10.1007/s13143-016-0011-2.

Kowalczyk, E., Stevens, L., Law, R., Dix, M., Wang, Y., Harman, I., Haynes, K., Srbinovsky, J., Pak, B., Ziehn, T., 2013. The land surface model component of ACCESS: description and impact on the simulated surface climatology. Aust. Meteorol. Oceanogr. J 63, 65–82.

Lemon, L.R., Stan-Sion, A., Soci, C., Cordoneanu, E., 2003. A strong, long-track, Romanian tornado. Atmos. Res. 67–68, 391–416. http://dx.doi.org/10.1016/S0169-8095(03)00063-2.

Lengfeld, K., Clemens, M., Merker, C., Münster, H., Ament, F., 2016. A simple method for

attenuation correction in local X-band radar measurements using C-band radar data. J. Atmos. Ocean. Technol. 33, 2315–2329. http://dx.doi.org/10.1175/JTECH-D-15-0091.1.
Lengfeld, K., Clemens, M., Münster, H., Ament, F., 2014. Performance of high-resolution X-band weather radar networks: the PATTERN example. Atmos. Meas. Tech. 7, 4151–4166. http://dx.doi.org/10.5194/amt-7-4151-2014.
Lipson, M.J., Hart, M.A., Thatcher, M., 2017. Efficiently modelling urban heat storage: an interface conduction scheme in an urban land surface model (aTEB v2.0). Geosci. Model Dev. 10, 991–1007. http://dx.doi.org/10.5194/gmd-10-991-2017.
Lompar, M., Curic, M., Romanic, D., 2017. Simulation of a severe convective storm using a numerical model with explicitly incorporated aerosols. Atmos. Res. 194, 164–177. http://dx.doi.org/10.1016/j.atmosres.2017.04.037.
Lompar, M., Curic, M., Romanic, D., 2018. Implementation of a gust front head collapse scheme in the WRF numerical model. Atmos. Res. 203, 231–245. http://dx.doi.org/10.1016/j.atmosres.2017.12.018.
Luhar, A.K., Thatcher, M., Hurley, P.J., 2014. Evaluating a building-averaged urban surface scheme in an operational mesoscale model for flow and dispersion. Atmos. Environ. 88, 47–58. http://dx.doi.org/10.1016/j.atmosenv.2014.01.059.
Marshall, J., Palmer, W.M., 1948. The distribution of raindrops with size. J. Atmos. Sci. 5, 165–166.
Marshall, T., Davis, W., Runnels, S., 2012. Damage survey of the Joplin tornado. In: Preprints, 26th Conf. on Severe Local Storms, Nashville, TN, Amer. Meteor. Soc, pp. 21. https://ams.confex.com/ams/26SLS/webprogram/Manuscript/Paper211662/Joplinmerger.pdf.
Masson, V., 2000, Mar, Mar. A physically-based scheme for the urban energy budget in atmospheric models. Bound.-Layer Meteorol. 94, 357–397. http://dx.doi.org/10.1023/A:1002463829265.
McGregor, J.L., 2003. A new convection scheme using a simple closure. In: Current issues in the parameterization of convection, pp. 33–36.
McGregor, J.L., 2005a. C-CAM: Geometric Aspects and Dynamical Formulation. CSIRO Atmospheric Research Dickson ACT.
McGregor, J.L., 2005b. Geostrophic adjustment for reversibly staggered grids. Mon. Weather Rev. 133, 1119–1128. http://dx.doi.org/10.1175/MWR2908.1.
McGregor, J.L., Dix, M.R., 2008. An Updated Description of the Conformal-Cubic Atmospheric Model. Springer New York, New York, NY, pp. 51–75. http://dx.doi.org/10.1007/978-0-387-49791-4_4.
Púčik, T., Groenemeijer, P., Rýva, D., Kolář, M., 2015. Proximity soundings of severe and nonsevere thunderstorms in Central Europe. Mon. Weather Rev. 143, 4805–4821. http://dx.doi.org/10.1175/MWR-D-15-0104.1.
Rotstayn, L.D., 1997. A physically based scheme for the treatment of stratiform clouds and precipitation in large-scale models. I: description and evaluation of the microphysical processes. Q. J. R. Meteorol. Soc. 123, 1227–1282. http://dx.doi.org/10.1002/qj.49712354106.
Rotstayn, L.D., Collier, M.A., Mitchell, R.M., Qin, Y., Campbell, S.K., Dravitzki, S.M., 2011. Simulated enhancement of ENSO-related rainfall variability due to Australian dust. Atmos. Chem. Phys. 11, 6575–6592. http://dx.doi.org/10.5194/acp-11-6575-2011.
Rotstayn, L.D., Lohmann, U., 2002. Simulation of the tropospheric sulfur cycle in a global model with a physically based cloud scheme. J. Geophys. Res. Atmos. 107http://dx.doi.org/10.1029/2002JD002128. AAC 20-1-AAC 20-21.
Schlünzen, K.H., Hoffmann, P., Rosenhagen, G., Riecke, W., 2010. Long-term changes and regional differences in temperature and precipitation in the metropolitan area of Hamburg. Int. J. Climatol. 30, 1121–1136. http://dx.doi.org/10.1002/joc.1968.
Schmidt, F., 1977. Variable fine mesh in the spectral global models. Beitr. Phys. Atmos. 50, 211–217.
Schwarzkopf, M.D., Ramaswamy, V., 1999. Radiative effects of CH4, N2O, halocarbons and the foreign-broadened H2O continuum: a GCM experiment. J. Geophys. Res. Atmos. 104, 9467–9488. http://dx.doi.org/10.1029/1999JD900003.
SPC, 2017. Storm Prediction Center Guidelines. http://www.spc.noaa.gov/exper/mesoanalysis/ last accessed 12.30.2017.
Stephan, K., Klink, S., Schraff, C., 2008. Assimilation of radar-derived rain rates into the convective-scale model COSMO-DE at DWD. Q. J. R. Meteorol. Soc. 134, 1315–1326. http://dx.doi.org/10.1002/qj.269.
Stratman, D.R., Brewster, K.A., 2017. Sensitivities of 1-km forecasts of 24 May 2011 tornadic supercells to microphysics parameterizations. Mon. Weather Rev. 145, 2697–2721. http://dx.doi.org/10.1175/MWR-D-16-0282.1.
Sutherland-Stacey, L., Shucksmith, P., Austin, G., 2010. High resolution observation of a small tornado, Ardmore, New Zealand. Weather Clim. 30, 49–56.
Tanamachi, R.L., Bluestein, H.B., Houser, J.B., Frasier, S.J., Hardwick, K.M., 2012. Mobile, X-band, polarimetric doppler radar observations of the 4 May 2007 Greensburg, Kansas, tornadic supercell. Mon. Weather Rev. 140, 2103–2125. http://dx.doi.org/10.1175/MWR-D-11-00142.1.
Tang, Y., Lean, H.W., Bornemann, J., 2013. The benefits of the Met Office variable resolution NWP model for forecasting convection. Meteorol. Appl. 20, 417–426. http://dx.doi.org/10.1002/met.1300.
Thatcher, M., Hurley, P., 2010. A customisable downscaling approach for local-scale meteorological and air pollution forecasting: performance evaluation for a year of urban meteorological forecasts. Environ. Model Softw. 25, 82–92. http://dx.doi.org/10.1016/j.envsoft.2009.07.014.
Thatcher, M., Hurley, P., 2012. Simulating australian urban climate in a mesoscale atmospheric numerical model. Bound.-Layer Meteorol. 142, 149–175. http://dx.doi.org/10.1007/s10546-011-9663-8.
Thatcher, M., McGregor, J.L., 2009. Using a scale-selective filter for dynamical downscaling with the conformal cubic atmospheric model. Mon. Weather Rev. 137, 1742–1752. http://dx.doi.org/10.1175/2008MWR2599.1.
Thompson, R.L., Edwards, R., Hart, J.A., Elmore, K.L., Markowski, P., 2003. Close proximity soundings within supercell environments obtained from the rapid update cycle. Weather Forecast. 18, 1243–1261. http://dx.doi.org/10.1175/1520-0434(2003)018<1243:CPSWSE>2.0.CO;2.
Thompson, R.L., Smith, B.T., Grams, J.S., Dean, A.R., Broyles, C., 2012. Convective modes for significant severe thunderstorms in the contiguous United States. Part II: Supercell and QLCS tornado environments. Weather Forecast. 27, 1136–1154. http://dx.doi.org/10.1175/WAF-D-11-00116.1.
Tornadoliste, 2017. Tornadoliste Deutschland. http://www.tornadoliste.de/read:5486 last accessed 12.30.2017.
Trapp, R.J., Stumpf, G.J., Manross, K.L., 2005. A reassessment of the percentage of tornadic mesocyclones. Weather Forecast. 20, 680–687. http://dx.doi.org/10.1175/WAF864.1.
Ulbrich, C., Atlas, D., 1978. The rain parameter diagram: methods and application. J. Geophys. Res. 83, 1319–1325.
Wurman, J., Gill, S., 2000. Finescale radar observations of the Dimmitt, Texas (2 June 1995), tornado. Mon. Weather Rev. 128, 2135–2164. http://dx.doi.org/10.1175/1520-0493(2000)128<2135:FROOTD>2.0.CO;2.